High mid-Holocene accumulation rates over West Antarctica inferred from a pervasive ice-penetrating radar reflector

Julien A. Bodart[1], Robert G. Bingham[1], Duncan A. Young[2], Joseph A. MacGregor[3], David W. Ashmore[4,5], Enrica Quartini[2,6], Andrew S. Hein[1], David G. Vaughan[7†], and Donald D. Blankenship[2]

[1]School of GeoSciences, University of Edinburgh, Edinburgh, UK
[2]Institute for Geophysics, University of Texas at Austin, Austin, Texas, USA
[3]Cryospheric Sciences Laboratory, NASA Goddard Space Flight Center, Greenbelt, Maryland, USA
[4]School of Environmental Sciences, University of Liverpool, Liverpool, UK
[5]Met Office, Exeter, UK
[6]Department of Astronomy, Cornell University, Ithaca, New York, USA
[7]British Antarctic Survey, Cambridge, UK
[†] Deceased

Correspondence to: Julien A. Bodart (julien.bodart@ed.ac.uk)

Key points

- We estimate mean accumulation rates for the past ~4700 years across the Pine Island, Thwaites, and Institute and Möller ice-stream catchments in West Antarctica using a ubiquitous, ice-core dated internal radar reflection
- Accumulation rates were 18% higher during the mid-Holocene compared to modern rates over the Amundsen-Weddell-Ross divide
- Spin-up of regional and continental ice-sheet models should include time-varying changes in Holocene accumulation rates from the WAIS Divide Ice Core to generate more realistic grounding-line evolution and past sea level rise contribution across this region

30   **Abstract**
31
32   Understanding the past and future evolution of the Antarctic Ice Sheet is challenged by the availability
33   and quality of observed palaeo-boundary conditions. Numerical ice-sheet models often rely on these
34   palaeo-boundary conditions to guide and evaluate their models' predictions of sea-level rise, with
35   varying levels of confidence due to the sparsity of existing data across the ice sheet. A key data source
36   for large-scale reconstruction of past ice-sheet processes are Internal Reflecting Horizons (IRHs)
37   detected by Radio-Echo Sounding (RES). When isochronal and dated at ice cores, IRHs can be used to
38   determine palaeo-accumulation rates and patterns therein. Using a spatially extensive IRH over Pine
39   Island Glacier, Thwaites Glacier, and Institute and Möller Ice Streams (covering a total of 610 000 km^2
40   or 30% of the WAIS), and a local layer approximation model, we infer mid-Holocene accumulation
41   rates over the slow-flowing parts of these catchments for the past ~4700 years. By comparing our results
42   with modern climate reanalysis models (1979 – 2019) and observational syntheses (1651 – 2010), we
43   estimate that accumulation rates over the Amundsen-Weddell-Ross divide were on average 18% higher
44   during the mid-Holocene than modern rates. However, no significant spatial changes in the
45   accumulation pattern were observed. The higher mid-Holocene accumulation-rate estimates match
46   previous palaeo-accumulation estimates from ice-core records and targeted RES surveys over the ice
47   divide, and they also coincide with periods of grounding-line readvance during the Holocene over the
48   Weddell and Ross Sea sectors. We find that our spatially-extensive, mid-Holocene-to-present
49   accumulation estimates are consistent with a sustained late-Holocene period of higher accumulation
50   rates occurring over millennia at the WAIS Divide Ice Core, thus highlighting the spatial
51   representativeness of this ice core to the wider West Antarctic region. We conclude that future regional
52   and continental ice-sheet modelling studies should base their climatic forcings on time-varying
53   accumulation rates from the WAIS Divide Ice Core through the Holocene to generate more realistic
54   predictions of the West Antarctic Ice Sheet's past contribution to sea-level rise.
55
56
57   **Key words:** West Antarctica, Internal Reflecting Horizons, Accumulation, Holocene, Ice-Penetrating
58   Radars, Ice-Core, Pine Island Glacier, Thwaites Glacier.
59

1. Introduction

Improving our knowledge of past climatic changes over the Antarctic Ice Sheet is required if we are to understand its present evolution and model its future under increasingly rapid climatic changes (IPCC, 2021). Most studies of past ice-sheet behaviour over Antarctica have focused on modelling changes in ice volume and grounding-line retreat following the Last Glacial Maximum (LGM, ~20 ka Before Present, BP) (Denton and Hughes, 2002; Golledge et al., 2012; 2013; Hillenbrand et al., 2013; 2014; Le Brocq et al., 2011; Kingslake et al., 2018); however, less attention has been paid to ice-sheet evolution during the Holocene (~11.7 ka BP to present). Recent evidence suggests that parts of the grounding line of West Antarctica may have retreated several hundred kilometres inland from its current position at ~10 ka and subsequently readvanced to reach its modern position sometime during the Holocene, due to isostatic rebound and climate-induced changes, particularly over the Weddell Sea and western Ross Sea sectors (Siegert et al., 2013; Bradley et al., 2015; Kingslake et al., 2018; Wearing and Kingslake, 2019; Venturelli et al., 2020; Neuhaus et al., 2021; Johnson et al., 2022). However, the atmospheric and ice-dynamical conditions farther inland, which could also have induced grounding-line migration, remain poorly constrained. An early investigation by Whillans (1976) using radar data near Byrd Ice Core indicated stability during the Late Pleistocene and Holocene epochs. Records of temperature and precipitation from the WAIS Divide Ice Core (hereafter abbreviated as WD14; Fig. 1) in the central West Antarctic Ice Sheet (WAIS) suggest higher accumulation rates during the Holocene than at present (Fudge et al., 2016), a trend that is also observed across small parts of the Amundsen-Weddell-Ross divide (Fig. 1) near the WAIS Divide Ice Core (hereafter referred to as WD14; Fig. 1) where isolated Radio-Echo Sounding (RES) surveys have shown 15-30% higher accumulation rates during the mid-Holocene compared to modern values (Siegert and Payne, 2004; Neumann et al., 2008; Koutnik et al., 2016).

Many numerical ice-sheet models that aim to predict Antarctica's long-term (past and future) contribution to sea-level rise use past ice-sheet reconstructions from after the LGM to guide and evaluate their models (Chavaillaz et al., 2013; DeConto and Pollard, 2016; Bracegirdle et al., 2019). However, even well-used ice-sheet reconstructions assume that the ice sheet retreated continuously throughout the Holocene (e.g. RAISED Consortium, 2014), a finding that has been challenged recently for the WAIS (e.g. Kingslake et al., 2018). Further, significant discrepancies between model simulations and the palaeo-proxy record currently impede our ability to predict confidently how the ice sheet will respond to future changes in the climate (e.g. Johnson et al., 2021). While improvements in model parameterisations are needed to close this gap (Bracegirdle et al., 2019; Sutter et al., 2021), considerable improvement in the availability and quality of palaeo-proxy records, particularly during the Holocene, is also needed to provide better constraints for ice-sheet models and ultimately better resolve past ice-sheet changes (Kingslake et al., 2018; Jones et al., 2022). Palaeo-proxy data have traditionally come from point-based measurements, such as ice cores (e.g. Petit et al., 1999; Parrenin et al., 2007; WAIS Divide Project Members, 2013; Buizert et al., 2021), sediment cores (e.g. Hillenbrand et al., 2013; Arnd et al., 2017; Hillenbrand et al., 2017; Kingslake et al, 2018; Venturelli et al., 2020; Neuhaus et al., 2021; Sproson et al., 2022), or surface-exposure dating (e.g. Stone et al., 2003; Suganuma et al., 2014; Johnson et al., 2014; Hein et al., 2016; Nichols et al., 2019; Johnson et al., 2020; Braddock et al., 2022). A complimentary and spatially extensive alternative data source for inferring past climate across an ice sheet is provided by Internal Reflecting Horizons (IRHs) detected by RES. They primarily result from englacial acidity contrasts and are often detected horizontally for hundreds of kilometres on RES data (Harrison, 1973; Bingham and Siegert, 2007). When employed in combination with ice-core stratigraphies, IRHs can be used to extend age-depth relationships away from an ice core by following peaks in electromagnetic power in the radar data (e.g. Beem et al., 2021; Bodart et al., 2021a; Cavitte et al., 2016; Jacobel and Welch, 2005; MacGregor et al., 2015; Whillans, 1976; Winter et al., 2019).

108   In contrast to East Antarctica and Greenland, IRH extension of WAIS ice cores has so far
109   been challenging due to fewer deep ice cores there and, until recently, the lack of well-dated IRH
110   datasets. However, efforts have intensified in recent years to improve our understanding of ice
111   stratigraphy over this sector. In particular, four recent studies using airborne RES data (Karlsson et al.,
112   2014; Muldoon et al., 2018; Ashmore et al., 2020a; Bodart et al., 2021a) all identified a distinct and
113   bright IRH dated using the Byrd and WD14 ice-core chronologies to 4.72 ± 0.28 ka BP (Muldoon et
114   al., 2018; Bodart et al., 2021a). A comparison of volcanic sulphate deposition within the WD14 and
115   Siple Dome ice cores revealed a large peak in sulphate concentration matching the age and depth of
116   this ubiquitous IRH (Kurbatov et al., 2006; Bodart et al., 2021a; Cole-Dai et al., 2021; Sigl et al.,
117   2022), which we hereafter term the "4.72 ka IRH". This IRH has now been observed by multiple RES
118   systems and extends throughout much of the slower-flowing ice of the Amundsen and Weddell Sea
119   embayments (< 400 m a^{-1}), including across the divides demarcating regions draining into the
120   Amundsen, Weddell and Ross Seas.

121   Despite their potential wide-ranging applications, the incorporation of IRHs into ice-sheet
122   models has so far been limited compared to other types of palaeo-proxy data, primarily because the
123   inference of accumulation-rate or ice-flow history from IRHs is an ill-posed inverse problem
124   (Waddington et al., 2007). Previous applications using IRHs to inform regional and continental
125   models include: (a) constraining decadal-scale Surface Mass Balance (SMB) estimates from
126   atmospheric models using annually-resolved IRHs found in the shallow firn (Medley et al., 2013;
127   2014; Van Wessem et al. 2018; Dattler et al., 2019; Kaush et al., 2020; Cavitte et al., 2022); (b)
128   inferring past accumulation rates going back further in time (i.e. 100s to 1000s years) with the aim of
129   comparing past accumulation estimates with modern times (e.g. Leysinger Vieli et al., 2004; Siegert
130   and Payne, 2004; Neumann et al., 2008; MacGregor et al., 2009; 2016; Leysinger Vieli et al., 2011;
131   Cavitte et al., 2018); or (c) integrating both their characteristics (e.g. elevation in the ice) and the
132   information inferred from them (e.g. accumulation or basal-melt rates) to evaluate the output from
133   regional and continental ice-sheet models (Leysinger Vieli et al., 2011; 2018; Holschuh et al., 2017;
134   Sutter et al., 2021). Promisingly, Sutter et al. (2021) recently showed that spatially extensive Antarctic
135   IRHs can provide unique benchmarks for constraining ice-sheet model parameterisations (i.e. climate
136   forcing and simulated ice flow), which are then used to simulate palaeo ice-sheet evolution. Together,
137   these studies indicate multiple avenues for ice-sheet models to assimilate IRHs further improve
138   estimates of past, current and future ice-sheet changes.

140   Here, we estimate mid-Holocene accumulation rates across the WAIS from first-order
141   calculations using a one-dimensional (1-D) model, constrained by the spatially extensive 4.72 ka IRH.
142   We first describe the data, the model used and their limitations and uncertainties (Sect. 2). We then
143   present our accumulation-rate estimates and compare to observed and modelled modern accumulation
144   rates to reveal a longer-term perspective on changes between the mid-Holocene and the present (Sect.
145   3). Finally, we place our results in the context of previous studies that consider WAIS evolution
146   during the Holocene (Sect. 4).

2. Data and methods

2.1 Along-track IRH data

150   We used data from extensive (~91 000 flight-track km) RES surveys acquired across West
151   Antarctica between 2004 and 2018. The main contributing surveys are the University of Texas
152   Institute for Geophysics (UTIG) 2004-2005 AGASEA survey flown over Thwaites Glacier (THW)
153   and Marie Byrd Land which deployed the 60-MHz High Capability Airborne Radar Sounder
154   (HiCARS) radar system (Holt et al., 2006; Peters et al., 2007), and the British Antarctic Survey (BAS)
155   2004-05 BBAS survey over Pine Island Glacier (PIG) and 2010-2011 IMAFI survey over Institute
156   and Möller Ice Streams (IMIS) which deployed the 150-MHz Polarimetric Airborne Survey
157   INstument (PASIN) radar system (Vaughan et al., 2006; Corr et al., 2007; Ross et al., 2012; Frémand,

158 Bodart et al., 2022) (Fig. 1; Table 1). Additional profiles from NASA's Operation Ice Bridge (OIB;
159 MacGregor et al., 2021) 2016 and 2018 surveys, flown with the 190-MHz Multichannel Coherent
160 Radar Depth Sounder 2 (MCoRDS-2) radar system (CReSIS, 2018), were also used to extract IRH
161 information near the WD14 Ice Core and upper IMIS catchments (Bodart et al., 2021a; Figure 1 and
162 Table 1). We refer the reader to the above references for comprehensive details on each system's
163 capabilities.
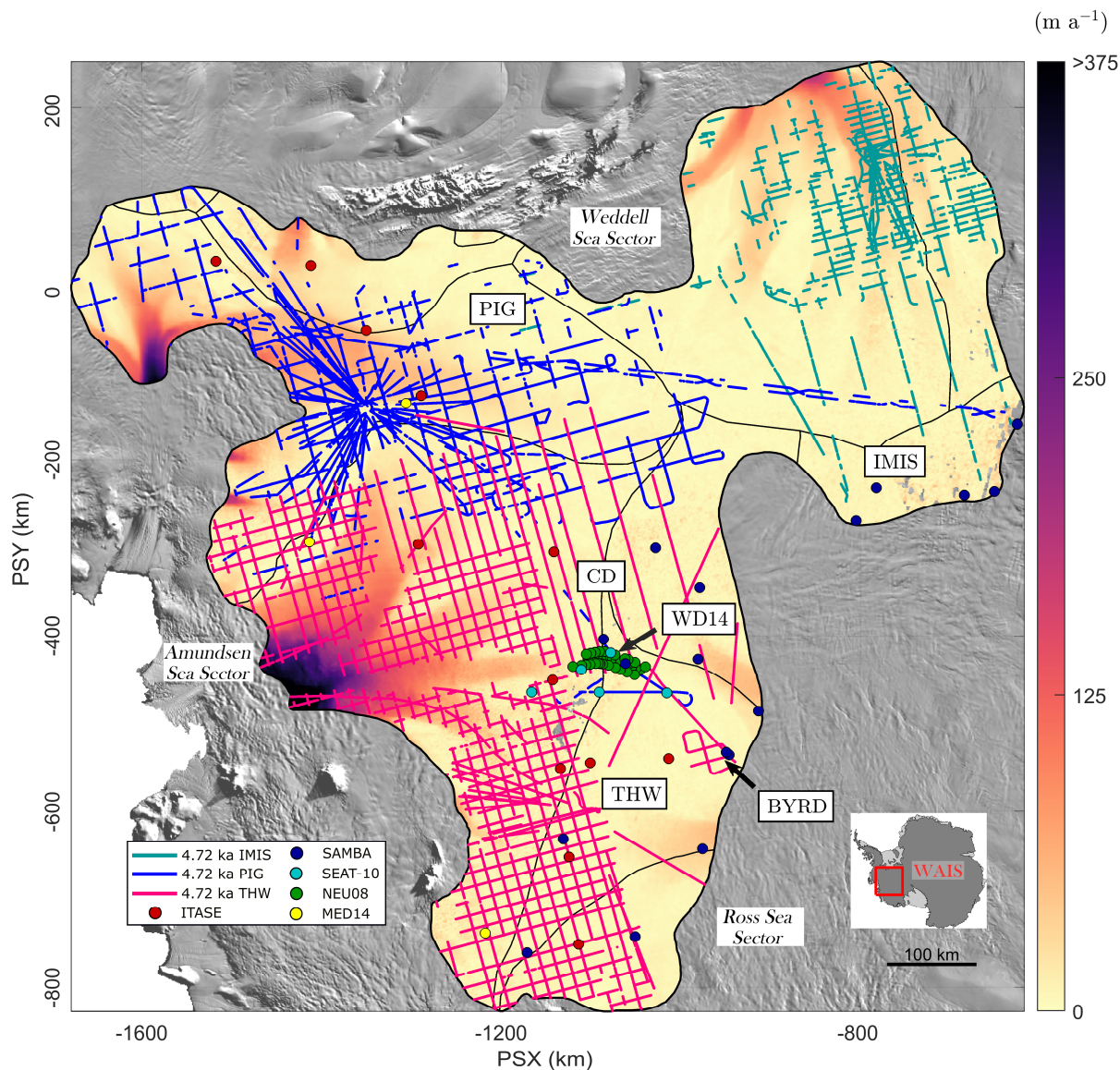
165 Figure 1. Map of the datasets and key locations in this study. The three datasets that contain the 4.72 ka
166 IRH are colour-coded as IMIS (green), PIG (blue), and THW (pink). IRH data where $D > 1$ are excluded (see
167 Section 2.2.1; Figure S1). Points represent the snow, firn and ice cores used in this study to compare modern
168 accumulation rates with those inferred from the 4.72 ka IRH (Sect. 2.4). The background colour map shows
169 modern surface speeds from Rignot et al. (2017). Locations mentioned in this paper are abbreviated on the map,
170 as follows: BYRD (Byrd Ice Core), IMIS (Institute and Möller Ice Streams), PIG (Pine Island Glacier), THW
171 (Thwaites Glacier), WAIS (West Antarctic Ice Sheet), CD (Central Amundsen-Weddell-Ross Divide), WD14
172 (WAIS Divide Ice Core). Major ice divides are from Mouginot et al. (2017). The background image is the 2014
173 MODIS mosaic of Antarctica (Haran et al., 2018). For all analysis and figures in this study, the SCAR Antarctic
174 Polar Stereographic projection is used (EPSG: 3031).

175 These RES surveys were used to track and date six IRHs spanning the Late Pleistocene and
176 Holocene (25.7 – 2.3 ka BP) that collectively cover much of the WAIS, including IMIS (Ashmore et

al., 2020a), PIG (Karlsson et al., 2014; Bodart et al., 2021a) and THW (Muldoon et al., 2018). Here
we only consider the 4.72 ka IRH mapped in all four studies and shown in Figure 1, as it is by far both
the most spatially extensive and the only commonly traced IRH across all studies. We first merged all
data points from the 4.72 ka IRH across the three catchments, resulting in a cumulative distance of
~40 000 line-km of IRH profiles (44% of the RES surveys' total coverage; Table 1). Although the
along-track RES data were acquired with a trace spacing of between 10 and 35 m, depending on the
dataset used, we re-sampled these points to 500 m in the along-track direction. We then added a
spatially invariant firn correction of 10 m onto the Muldoon et al. (2018) dataset to match the same
firn correction applied by the other studies to correct the IRH depth. Finally, we calculated the median
value of all ice thicknesses and IRH depths falling within each 500 m interval.

Table 1. Characteristics of each IRH dataset used in this study that contain the 4.72 ka IRH. 'Reflector
1' in Muldoon et al. (2018) is abbreviated here as 'R1'.

Survey name	Survey provider	RES system	Dataset reference	Cumulative IRH distance (10^3 km)
IMAFI	BAS	PASIN 150-MHz	H2 in Ashmore et al. (2020a)	15
BBAS / OIB	BAS / NASA	PASIN 150-MHz / MCoRDS-2 190-MHz	R2 in Bodart et al. (2021a)	6
AGASEA	UTIG	HiCARS 60-MHz	R1 in Muldoon et al. (2018)	19

2.2 Inferring accumulation rates

To infer accumulation rates from the 4.72 ka IRH, we used the Nye model, a 1-D ice-flow
model widely used for estimating accumulation rates and age-depth relationships over relatively slow-
flowing parts of an ice sheet (Nye, 1957; Fahnestock et al., 2001a). This model invokes the local-layer
approximation (LLA), i.e. it assumes that the time-averaged accumulation rate that the IRH has
experienced since its upstream inception at the surface can be adequately represented by its depth
where it is observed presently. Other 1-D models exist, including the Dansgaard-Johnsen (Dansgaard
and Johnsen, 1969) and the shallow-strain rate model (MacGregor et al., 2016), but were less suitable
for estimating accumulation rates here due to uncertainty in the basal shear layer thickness across our
survey area and because we are limited to only one IRH to constrain the ice-flow model respectively.
The Nye model assumes that ice thickness is constant and therefore that the ice sheet has been in a
steady state since the deposition of the IRH, an acceptable assumption for the period under
investigation here. The Nye model states:

$$\dot{b}_a = \ln\left(\frac{z_a}{H}\frac{H}{a}\right), \tag{1}$$

where $\dot{b}_a$ is the mean accumulation rate during the Holocene epoch between an IRH of age a and the
present, z_a represents the depth of the IRH dated at the ice core, and H is the ice thickness. The model
assumes that the vertical strain rate, $\dot{\varepsilon}_a$, is also constant and vertically uniform, so that it exactly
balances the overburden of local ice accumulation:

$$\dot{\varepsilon}_{zz}^a = \frac{\dot{b}_a}{H}. \tag{2}$$

We iterated Eq. (1) over the re-sampled 500-m spaced dataset using the depth of the 4.72 ka
IRH for z_a and used the median radar-derived ice-thickness measurement re-sampled over the 500-m
grid to obtain H, when this information was available. In areas where the radar did not sound the bed,

211 we used the BedMachine Antarctica v2 gridded product to obtain a value for H (Morlighem, 2020).
212 Note that accumulation rate values presented in this study are all reported in m a^{-1} of ice equivalent.

2.2.1 Assessing the suitability of the 1-D model

214 To quantify the suitability of the LLA from which our accumulation rates are based, we
215 calculated the effects of horizontal gradients in modern ice thickness and accumulation rates along
216 particle paths in their ability to affect IRH depths across our grid, as per Waddington et al. (2007).
217 Where these gradients are large, estimates of accumulation rates from IRHs likely require a more
218 complete treatment of ice flow and its effect upon IRH depths, which multi-dimensional models and
219 more physically complete models can better resolve (e.g. Waddington et al., 2007; Leysinger Vieli et
220 al., 2011; Karlsson et al., 2014; Nielsen et al., 2015; Koutnik et al., 2016;). However, such models are
221 significantly more computationally expensive over such a larger area and depend on well-constrained
222 boundary conditions from along-flow radar profiles which are not often available at an ice-sheet level
223 (MacGregor et al., 2009).

224 We quantified the effect of horizontal gradients on an IRH of age a by first estimating the
225 total horizontal particle path length L_{path} each "particle" of the 4.72 ka IRH has travelled since a, and
226 then the characteristic lengths of variability in ice thickness (L_H) and apparent accumulation rate ($L_{\dot{b}}$)
227 (Supplementary Information). These three components were then combined to generate a non-
228 dimensional parameter D (Fig. S1d), which we used as a confidence metric for our inferred
229 accumulation rates. Both Waddington et al. (2007) and MacGregor et al. (2009) suggested a value of
230 $D \ll 1$ over Antarctica, whereas MacGregor et al. (2016) used a maximum value of $D = 1$ to estimate
231 where the LLA is acceptable over Greenland. Because D cannot be translated simply into an
232 uncertainty in an LLA-inferred accumulation rate, it is not yet clear what exact value is appropriate.
233 Smaller values of D indicate that local horizontal gradients in ice thickness and accumulation rates
234 have a smaller effect on IRH depth of age a, and thus that the LLA may be valid (Waddington et al.,
235 2007; MacGregor et al., 2009; 2016). Where $D \geq 1$, the depth of an IRH is less likely to be the result
236 of accumulation rates at the surface or vertical strain rates further down, and thus a more sophisticated
237 model is likely required (Sect. 2.2.2) (Waddington et al., 2007). However, MacGregor et al. (2009)
238 found that even along a flowband across Lake Vostok where the mean value of D is 0.50 for a 41-ka
239 IRH, the difference in accumulation rate inferred from the LLA and from a more sophisticated
240 flowband model could be relatively small (4-16%). This similarly suggests that accumulation rate can
241 be inferred acceptably using the LLA where D is higher.

242 For our study area, D values are mostly well below unity (median: 0.19; 25th quartile: 0.09;
243 75th quartile: 0.34), which suggests relatively little effect from ice-dynamical processes upon IRH
244 depths across most of our grid. We used the upper quartile of the D distribution across our model
245 domain (i.e. $D \leq 0.34$) to show areas where we can have confidence that accumulation rate remains
246 the dominant factor influencing the vertical position of our IRHs in the ice column (i.e. where the
247 $D \ll 1$ criterion is likely met; Fig. S1d). While accumulation rates inferred from IRHs situated in the
248 upper quartile (Fig. S1d) may still be valid, we suggest additional caution in interpreting our results
249 there due to the potential impact of larger flow gradients on IRH depths.

2.2.2 Model limitations and uncertainty

251 One of the main limitations of the Nye model is that it assumes that gradients in sliding
252 velocity are mostly concentrated in a thin layer at the ice-bed interface and that the ice column
253 deforms by pure shear only (Nye, 1957; Fahnestock et al., 2001a). For this reason, the Nye model is
254 generally only appropriate for IRHs found in the upper part of the ice column, as is the case here.
255 Additionally, the use of the model is restricted to areas where ice flow is relatively slow and
256 horizontal strain rates are also relatively low.

257   Here we focus on a shallower IRH situated in the upper part of the ice column (median: 40%;
258 25th quartile: 30%; 75th quartile: 50%; Fig. 2b-c), for which we can reasonably assume that the ice
259 sheet has remained close to steady state and where IRHs are likely shallow enough not to have
260 experienced appreciable flow disturbances that would affect the Nye model assumptions.
261 Additionally, due to the inherent nature of tracking IRHs through RES data, our coverage is limited to
262 areas where ice-flow speeds are relatively low and IRHs are undisturbed. In some portions of our
263 study area, the IRH is found deeper in the ice column or in faster-flowing sections of the ice sheet
264 (e.g. in the downstream sectors of our grid, Fig. 1-2b-c); areas where the assumptions that the 1-D
265 model is based on may be challenged.

266   Estimating uncertainty in accumulation rates from the Nye model is non-trivial. Previous
267 studies have used the misfit between the accumulation rate calculated using multiple proximal IRHs
268 in the ice column (e.g. Fahnestock et al., 2001a; 2001b; Leysinger Vieli et al., 2004; MacGregor et al.,
269 2016). Unfortunately, this method is not suitable here due to the dearth of spatially extensive IRHs
270 younger than 4.72 ka over our model domain.

271   Instead, uncertainty in the Nye-inferred accumulation rates were calculated using: (a) the
272 lowest and highest possible accumulation rates from Eq. (1) using the age uncertainty (± 0.28 ka) of
273 the 4.72 ka IRH and (b) the lowest and highest possible accumulation rates inferred from an additional
274 1-D model (Eq. S5) which accounts for the effect of strain rates on accumulation rates (i.e. the
275 shallow-strain rate model from MacGregor et al. (2016); Supplementary Information; Fig. S2-4).

276   This calculation provides lower and upper bounds for the IRH-inferred accumulation rates
277 (Fig. S4a-b), which were then averaged to generate a relative uncertainty (Fig. S4c). From this
278 assessment, we estimate a median relative uncertainty in the Nye-inferred accumulation rates for the
279 4.72 ka IRH of 14% across our grid. This uncertainty is higher in the downstream edges of our grids,
280 particularly over the PIG, THW and IMIS catchments, and generally low over the Amundsen-
281 Weddell-Ross divide (Fig. S4), reflecting the effect of spatially variable strain rates on the inferred
282 accumulation rates. When combined with the assessment of the suitability of the LLA and exclusion
283 of IRHs where the $D > 1$ (Sect. 2.2.1-2.2.2), we conclude that it supports our application of a 1-D
284 modelling approach here.

2.3 Gridding and filtering

286   Once IRH depths and accumulation rates for the 4.72 ka IRH were obtained at regular 500-m
287 points along RES flight paths, we filtered the results using a moving-average Gaussian filter of length
288 30 samples (equivalent to ~15 km) to reduce along-track noise in the IRH depth, and then gridded the
289 filtered result using a Delaunay-triangulation-based natural neighbour interpolation method onto a 1-
290 km polar stereographic grid. We further smoothed the gridded data using an 18-km square cell mean
291 filter to limit the localised interpolation artefacts in areas of poor survey coverage. Figure S5 shows
292 the maximum distance away from the nearest 500-m along-track point used to produce Figures 2-3,
293 and thus where errors in the interpolated grids are expected to be larger. The median value of this
294 maximum distance is 5 km and its maximum value is 75 km, which is comparable to previous studies
295 that infer SMB from IRHs in the shallow firn (e.g. Medley et al., 2014). We evaluated other possible
296 interpolation methods (e.g. kriging and using different semi-variogram models), but they resulted in
297 similar or poorer quality and were thus discounted.

2.4 Comparison with modern observations

299   To compare our inferred accumulation estimates for the past 4.72 ka with modern values
300 (defined here as 1651-2019), we derived information on modern accumulation rates from two sources,
301 one modelled (gridded) and one from a series of observational (point-based) datasets.

302   We used modelled gridded accumulation rates from the Regional Atmospheric Climate Model
303   2.3p2 (hereafter RACMO2) 1979-2019 SMB product forced at its margin with the ERA-Interim
304   product (native resolution: 27 km) as an estimate for modern accumulation rates (Van Wessem et al.,
305   2018). Although SMB is not technically equivalent to the accumulation rate, runoff and sublimation
306   are negligible in our survey area (Medley et al., 2013) so we assume SMB is equal to accumulation
307   rate in this region. We converted modelled values from $kg\ m^{-2}\ a^{-1}$ to $m\ a^{-1}$ of ice equivalent using an
308   ice density value of 917 $kg\ m^{-3}$, calculated the 40-year mean, and then bi-linearly interpolated the
309   gridded RACMO2 product to the same 1-km grid resolution as our 4.72 ka-to-present accumulation
310   grid (Sect. 2.3) to ensure consistency when comparing both datasets.

311   Observational point-based measurements were obtained from a series of snow, firn and ice
312   cores from the ITASE (Mayewski and Dixon, 2013), MED14 (Medley et al., 2014), SAMBA (Favier
313   et al., 2013), and SEAT-10 (Burgener et al., 2013) datasets, as well as from a network of centennially-
314   averaged modern accumulation rates derived from shallow IRHs traced on ground-based RES data
315   over the central divide and dated using a shallow ITASE Ice Core (Neumann et al., 2008) (Fig. 1).
316   This resulted in 79 point-based accumulation measurements from cores covering the period 1651-
317   2010 CE (Common Era) and spread across our model domain (see Figure 1). Further detail on these
318   datasets can be found in the above references.

319   To compare the Holocene gridded product with the point-based measurements, we first
320   calculated the average value of the accumulation rate at the point measurement for the entire period.
321   We converted these values to ice-equivalent accumulation rates and then extracted two paired values,
322   i.e. the value for the point-measurement for modern accumulation rates and the value for the nearest
323   grid cell in the gridded 4.72 ka-to-present accumulation estimates to this measurement.

Results

325   The final grids for depth and accumulation rates for the 4.72 ka IRH are shown in Figures 2 and 3.
326   In total, these grids are made of ~89 000, 500-m spaced points, which cover an area of ~610 000 km^2,
327   or ~30% of the total surface area of the WAIS. The grids span most of the PIG and THW glacier
328   catchments, as well as the Ronne (upper Rutford, Institute, and Möller) and upper western Ross
329   (Bindschadler, Kamb, MacAyeal, and Whillans) catchments (IPY Antarctic boundaries G-H, J-Jpp,
330   and Ep-F; Mouginot et al. (2017); Fig. 1-2). Overall, the 4.72 ka IRH is shallower within the IMIS
331   and upper PIG and THW catchments, as well as on the Ross side of the central divide where ice
332   thickness is particularly deep (Fig. 2b). Conversely, the 4.72 ka IRH is deeper in the ice near a 400-m
333   high bedrock plateau that separates the northern and southern basins of PIG (Vaughan et al., 2006)
334   and at two locations in the upstream parts of the main trunk of THW where ice flows over highs in
335   subglacial topography (Fig. 2b).
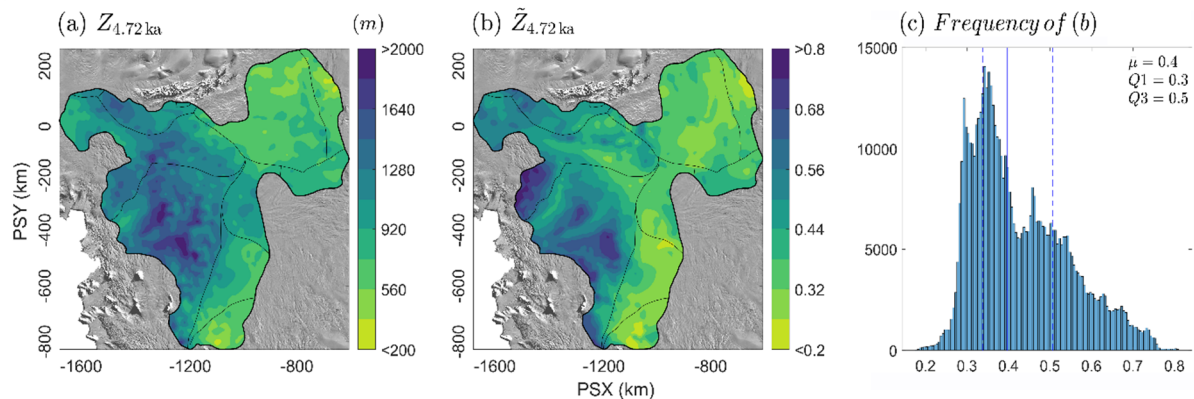
336

337   Figure 2. Gridded depths for the 4.72 ka IRH across the model domain covering the PIG, THW, and
338   Institute and Möller ice-stream catchments. (a) Gridded depth of the 4.72 ka IRH. (b) Normalised depth of the

4.72 ka IRH relative to ice thickness. (c) Histogram showing the distribution of values in (b) with the median ($\tilde{\mu}$) and interquartile range (i.e. 25th (Q1) and 75th (Q3) quartiles) shown as solid and dashed blue lines respectively. The background image is the 2014 MODIS mosaic of Antarctica (Haran et al., 2018).

3.1. Catchment-scale accumulation estimates

Figure 3 shows a comparison of the ice-equivalent accumulation rates we inferred for the 4.72 ka IRH (Fig. 3a) and modern SMB estimates from RACMO2 (Fig. 3b). We observe that the IRH accumulation rate pattern for the last 4.72 ka is similar to the modern pattern of accumulation rates for the Amundsen Sea sector of the WAIS, which is dominated by higher coastal accumulation rates that progressively decrease inland to reach their lowest rates over the Ross side of the divide (Fig. 3a-b). Differences in accumulation rates between the 4.72 ka-to-present estimates and modern values are mainly observed directly upstream of the main trunks of PIG and THW, where modern rates are much higher (up to 0.2 m a^{-1} ice equivalent) than for the 4.72 ka-to-present estimates (Fig. 3c). In comparison, higher accumulation rates for the last 4.72 ka relative to modern rates are observed for the entire stretch of the Amundsen-Weddell-Ross divide (Fig. 3c; Table 2). Over the IMIS catchment, little change is observed between the two periods. Over the entire model domain, we observe a median percentage change value of 6% higher accumulation since 4.72 ka compared with modern rates (Fig. 4); however, when considering only the values that fall within 100 km of either side of the Amundsen-Weddell-Ross divide (i.e. in the accumulation zone of the Amundsen, Weddell, and Ross Sea sectors and where mean surface speeds average ~7 m a^{-1}), we obtain a median percentage change value of 18% higher accumulation compared with modern accumulation rates (Fig. 4).
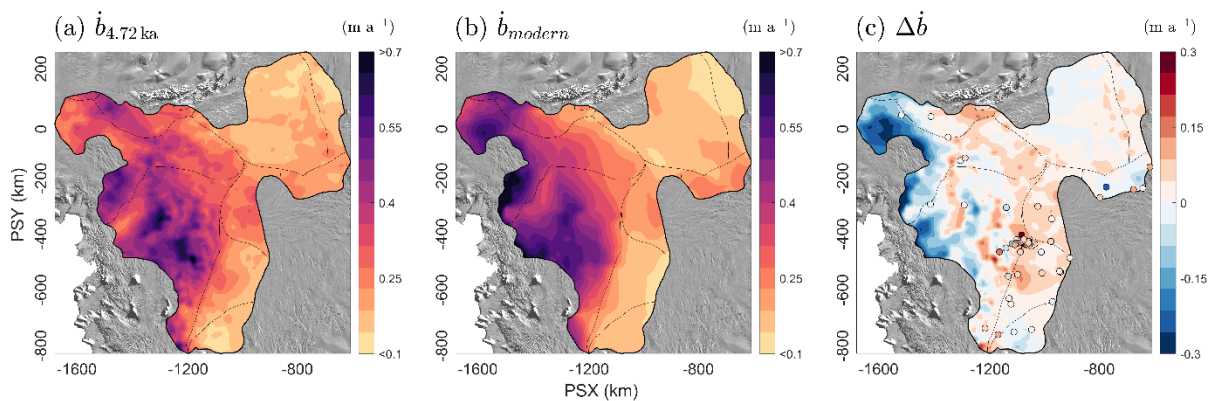
Figure 3. Gridded estimates of ice-equivalent accumulation rates for the last 4.72 ka and modern times. (a) Gridded accumulation rates inferred from the 4.72 ka IRH. (b) Modern (1979 – 2019) modelled SMB rates from RACMO2. (c) Difference between 4.72 ka-to-present and modern accumulation rates (red = 4.72 ka-to-present accumulation higher than modern times, blue = 4.72 ka-to-present accumulation lower than modern times). The dots represent the difference between the value for the nearest grid cell in (a) and time-averaged accumulation rates at each of the 79 core locations (see Section 2.4; Fig. S6). The background image is the 2014 MODIS mosaic of Antarctica (Haran et al., 2018).

Comparison between our 4.72 ka-to-present accumulation-rate estimates and 79 core-derived point-based accumulation measurements for modern times (1651-2010 CE) are shown in Figures 3-4 and S6. This evaluation shows that the 4.72 ka-to-present accumulation-rate estimates for the nearest grid cell to each point measurement are, on average, 22% higher for cores situated across the entire grid ($p < .0015$, n=79) and 23% higher for cores found within 100 km of the divide compared with modern accumulation rates ($p < .0001$, n=59; Figs. 4 and S6). In comparison, a similar analysis between grid cells from the 4.72 ka-to-present accumulation-rate estimates and RACMO2 at these 79 core locations shows mid-Holocene accumulation rate estimates are, on average, 32% ($P < .00002$, n=79) higher for cores situated across the entire grid and 36% higher for cores found within 100 km of the divide ($p < .00001$, n=59; Fig. S6). This result confirms that the relative change for gridded

accumulation rates between the 4.72 ka-to-present and modern modelled accumulation rates is consistent with modern rates from point-based measurements.

Table 2. Summary statistics for the modern (modelled and observational) and 4.72 ka-to-present ice-equivalent accumulation rates at the catchment-scale and over the Amundsen-Weddell-Ross divide (abbreviated CD here). Values for the Amundsen-Weddell-Ross divide are for all points that fall within 100 km of either side of the divide (see dashed line in Figure 4). $\tilde{\mu}$ refers to the median and IQR represents the Interquartile Range calculated by computing the difference between the 75th and 25th percentiles. Note that the values provided in the text represent the median relative change from the cell-by-cell change between each grid (Fig. 4), rather than the relative change of the median values provided here.

Accumulation rate (m a⁻¹)	Catchment-wide		CD only	
	$\tilde{\mu}$	IQR	$\tilde{\mu}$	IQR
Modern (model)	0.23	0.23	0.22	0.10
Modern (cores)	0.24	0.12	0.24	0.09
4.72 ka-to-present	0.27	0.18	0.27	0.11
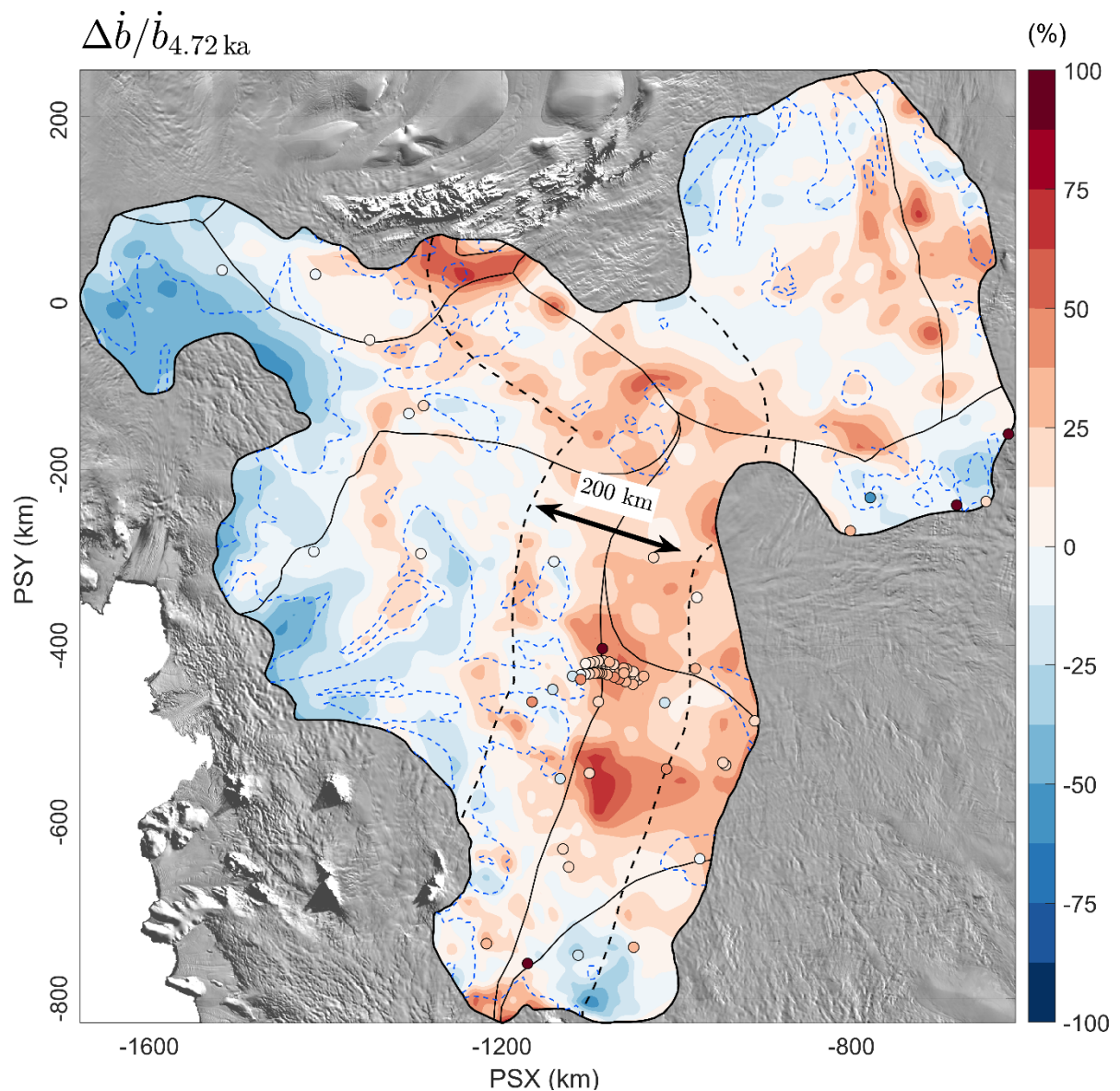
Figure 4. Relative change in accumulation rates between the 4.72 ka-to-present estimates and modern rates. The points on the map represent the relative change in ice-equivalent accumulation rate between the nearest grid cell in the 4.72 ka-to-present grid and the 79 modern observations from cores (Figs. 1 and S6; Sect. 2.4). The dashed black outline line represents the 100-km boundary on either side of the Amundsen-Weddell-Ross divide used to provide the summary statistics in Section 3.1 and Table 2. The dashed blue line shows the contours of the upper limit of the interquartile range for the D parameter ($D \leq 0.34$) (Sect. 2.2.1-2.2.2). The background image is the 2014 MODIS mosaic of Antarctica (Haran et al., 2018).

3.2 Elevation-dependent accumulation estimates

While Figures 3 and 4 help to assess potential differences in patterns and rates across spatial scales, considering accumulation-rate differences in terms of elevation can inform how topography influences accumulation and whether this has changed over time. We binned the ice-equivalent accumulation values by 50-m elevation bands across the three main catchments covering our grid (Amundsen, Weddell and Ross) for both the 4.72 ka-to-present estimates and modern model rates and calculated the mean accumulation rate and the total accumulation rate for each bin over the entire elevation gradient (Fig. 5). We again find that the accumulation-rate estimates for the period since 4.72 ka are lower at low elevations (~700 – 1400 m) over the Amundsen sector compared with RACMO2, but begin to exceed RACMO2 near the 1400-m elevation band where the 4.72 ka-to-present accumulation rate is higher than modern times across the divide (Fig. 5a-b). We also note that whilst an elevation-dependent gradient in accumulation rates, dominated by high accumulation at the coast decreasing inland, exists over this sector for the mid-Holocene, it is much less marked than for present rates. This is not surprising, as this sector is where we observe the largest relative uncertainties in inferred accumulation rates across our grid (Fig. S4), indicating that the 1-D model is less able to produce realistic accumulation rates in the downstream end of our grid where ice flow is faster and strain rates are likely higher. In comparison to the Amundsen sector, accumulation rates since 4.72 ka are generally higher at all elevations for the Weddell and Ross sectors compared with the present, although this difference is less than over the Amundsen sector (Fig. 5 c-f).
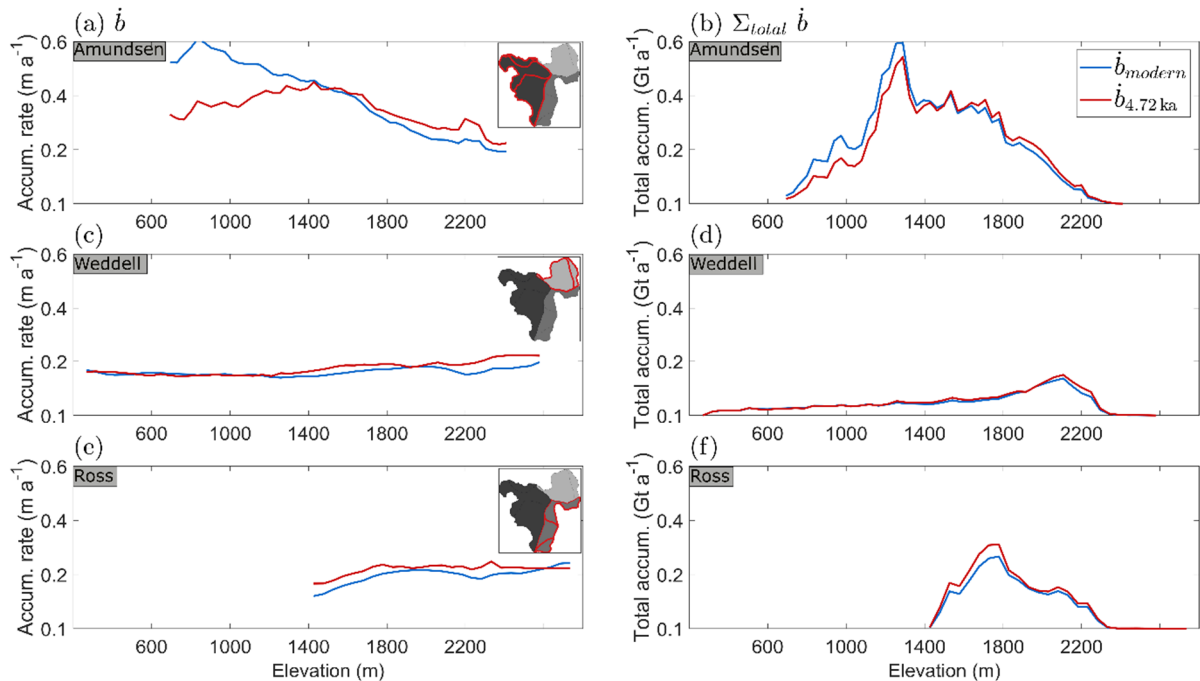
Figure 5. Comparison of ice-equivalent accumulation rates between the 4.72 ka-to-present estimates and modern rates (RACMO2) binned by 50-m elevation bands across the three main catchments considered here (Amundsen, Weddell, and Ross). (a, c, e) Mean accumulation rate averaged per 50-m elevation band across the specific catchment area in m a^{-1}. (b, d, f) Total accumulation rate per 50-m elevation band across the specific catchment area in Gigatonnes per annum (Gt a^{-1}).

4. Discussion

4.1. Comparison with other Holocene accumulation estimates

Previous studies of past accumulation rates over the WAIS have shown that accumulation varied temporally during the Holocene. Using a single airborne RES profile over the Amundsen Sea sector, Siegert and Payne (2004) showed that accumulation rates were approximately the same at 3.1 ka compared with modern rates, but ~0.3 m a^{-1} greater (~15 %) than current rates between 3.1-6.4 ka, before which accumulation was ~50% of modern rates between 6.4 and 16.0 ka. Similarly, Neumann et al. (2008) found that accumulation rates at the Amundsen-Weddell-Ross divide were ~30% higher between 3-5 ka than modern values based on a dense network of IRHs traced on ground-based RES data, while Karlsson et al. (2014) found that accumulation patterns had likely changed twice during the early to mid-Holocene over PIG from the lack of a model fit between the depths and ages of two prominent IRHs. Using the updated WD14 record, Fudge et al. (2016) showed that accumulation rates were higher there in the mid to late-Holocene (19% between 4.72 ka BP and the present), a trend that was also observed by Koutnik et al. (2016), who found a 20% increase in accumulation rates between 2-4 ka compared with modern rates from a ground-based RES profile across the ice divide.

These studies together point to a period of increasing accumulation observed at the WD14 Ice Core from ~7 ka onwards (Fudge et al., 2016; their Figure 2), with its peak matching the age of the 4.72 ka IRH used here. Thus, our accumulation-rate estimates likely form part of a wider pattern of a sustained increase in accumulation across the Amundsen-Weddell-Ross divide over several millennia. In showing that mean accumulation rates since 4.72 ka were 18% greater than modern rates modelled from RACMO2 across the Amundsen-Weddell-Ross divide, our results provide much wider regional support for the hypothesis that accumulation rates during the mid-Holocene exceeded modern rates across central West Antarctica. A possible explanation for the higher accumulation rates during the mid-Holocene compared with modern values is that they represent a continued climatic transition from the LGM (Steig et al., 2001). Alternatively, it has been suggested that seasonal or interannual variability, such as a weaker circumpolar vortex (van Den Broeke and van Lipzig, 2004; Neumann et al., 2008), or teleconnections to tropical Pacific Ocean warming (Sproson et al., 2022), may also lead to such difference. We did not find evidence for significant changes in accumulation patterns between the mid-Holocene and modern times, suggesting that the current spatial pattern of high accumulation on the Amundsen side of the divide transitioning to low accumulation on the Ross side of the divide was stable throughout the mid-Holocene, as previously suggested by others (Siegert and Payne, 2004; Neumann et al., 2008; Koutnik et al., 2016).

We also find that accumulation estimates for the 4.72 ka-to-present are smaller than modern rates in the lowest elevation bands (<1400 m), particularly over the Amundsen Sector (Fig. 5 a-d). This pattern was also found by Medley et al. (2014), who compared modern observational and modelled data over this sector and hypothesised that this discrepancy at low elevations resulted primarily from a lack of sufficient accumulation measurements in the lower sections of their survey area. In our case, these low-elevation values are close to the boundary where we consider the LLA acceptable for the 4.72 ka IRH, albeit where D values are higher than for the rest of the catchment (Figure S1d), so it is more likely that accumulation rates calculated there are affected by ice-flow gradients and their influence upon IRH depths leading to lower accumulation rates there. Despite this caveat, Figures 5b and 5d show that values at low elevations contribute relatively little to the total accumulation (by mass) over our survey area.

We suggest that future ice-sheet modelling studies investigate the difference in accumulation rates inferred from our 1-D model using multi-dimensional flowband models to assess effects of divergent and convergent flow on IRH depth and ultimately accumulation rates, as previously considered elsewhere in Antarctica (MacGregor et al., 2009). This could be conducted along a flowline transitioning from the slow-flowing regions directly downstream of the Amundsen-Weddell-Ross

468 divide to the coastal margins of our grid, particularly over THW where we observe the largest
469 uncertainties in accumulation rates. In addition, we suggest that future modelling studies use the
470 accumulation-rate variability from the WD14 Ice Core as a climate forcing in their ice-sheet models.
471 Koutnik et al. (2016) previously showed that the WD14 record is unique in that it provides a reliable
472 record of accumulation-rate variability during the Holocene, which other East Antarctic ice-core
473 records often used to reconstruct the evolution of the WAIS do not possess. We found that these
474 higher accumulation rates are spatially extensive across nearly one third of the WAIS, further
475 suggesting that the WD14 Ice Core is indeed representative of the wider WAIS and can be used in
476 regional or continental ice-sheet models as a reliable climate forcing for the region. Future regional
477 and continental ice-sheet models should make use of this record to adjust their climatic boundary
478 conditions to provide improved estimates of ice-elevation change and grounding-line evolution over
479 Antarctica.

480 **4.2 Impact for ice-sheet elevation change during the Holocene**

481 Model results from Steig et al. (2001) suggest that the maximum elevation of the WAIS was most
482 likely reached during the early to mid-Holocene (around ~7 ka) following higher accumulation rates
483 at the late glacial–interglacial transition, after which the WAIS slowly declined to present conditions
484 as the sea-level-rise-induced kinematic wave reached the ice-sheet interior and outpaced the increase
485 in accumulation rates. However, higher accumulation rates in the mid-Holocene relative to the
486 present, which our results suggest occurred spatially across the WAIS, would likely delay the timing
487 of this thinning by several thousand years (Steig et al., 2011).

488 Using a flowband model, Koutnik et al. (2016) suggested that an increase of up to 40% in
489 accumulation rates for the period 9 – 2 ka would likely have led to an increase in ice thickness of tens
490 of metres during the mid-Holocene. Although this finding was warranted by physical assumptions
491 around the response time of the ice-sheet interior to adjust to an increase in accumulation in the
492 model, it points to the potential for the divide to have thickened by several metres over a relatively
493 short period of time from increased accumulation rates alone. Because the WAIS is also sensitive to
494 ice-dynamical changes at the ice-sheet margins (e.g. grounding-line retreat or calving), an increase in
495 accumulation rates in the upper part of the ice sheet may not necessarily result in enough thickening to
496 counteract potential dynamical losses farther downstream (Jones et al., 2022). Conway and
497 Rasmussen (2008) reported that the Amundsen-Ross Divide is currently thinning and migrating
498 towards the Ross Sea at a speed of 10 m a^{-1}, but they were unable to determine whether this was in
499 response to long-term (last two millennia) accumulation-rate changes there or short-term (last few
500 centuries) ice-dynamical forcing from the coastal margins of the Amundsen and Ross sectors. More
501 recently, Balco et al. (2023) showed that Thwaites and Pope glaciers experienced 35 m of thickening
502 in the mid-to-late Holocene, when accumulation rates were higher than present. While this thickening
503 relative to present was attributed to glacio-isostatic rebound, it is also possible that higher
504 accumulation rates in the upstream sections of the WAIS contributed to this thickening, if sustained
505 over millennia.

506 The lack of an ice-dynamical component in the model used here precludes us from evaluating
507 any ice-surface-elevation change associated with changing accumulation rates. However, 18% higher
508 accumulation rates during the mid-Holocene relative to the present across 30% of the WAIS could be
509 consistent with an elevation increase of several tens of metres in ice thickness, according to Koutnik
510 et al. (2016). Even if tens of metres of ice-surface-elevation change occurred, it is still unlikely to
511 significantly affect the steady-state assumption of the 1-D model used here (constant ice thickness
512 over time), because such changes are small (a few per cent of the ice thickness) and that ice thickness
513 exceeds 3500 m in places over our survey area.

514 **4.3 Impact for grounding-line evolution during the Holocene over the WAIS**

Finally, we consider the possibility for Holocene ice thickening at the divide from increased accumulation rates to affect downstream grounding-line evolution. Recent evidence from ice-sheet modelling and field measurements suggest that grounding-line retreat during the Holocene was not monotonic, particularly at the Ross and Weddell Sea sides of the WAIS (Bradley et al., 2015; Kingslake et al., 2018; Neuhaus et al., 2021). Rather, Kingslake et al. (2018) showed that the grounding-line position in the Ross and Weddell Sea sectors initially retreated from the LGM inland until ~10.2 – 9.7 ka, and then readvanced to its modern position sometime during the Holocene. Although they attributed this change in grounding-line position to the solid Earth viscoelastic response due to ice-sheet mass change and the subsequent re-grounding around pinning points, it has also been suggested that an increase in accumulation rates upstream of the grounding line could lead to a readvance via ice thickening there and a subsequent increase in ice flow (Steig et al., 2001; Koutnik et al., 2016; Jones et al., 2022). Across parts of the Weddell Sea Embayment, several studies have produced evidence for stability of the LGM ice thickness there until the early to mid-Holocene (Ross et al., 2011; Hein et al., 2016; Ashmore et al., 2020a), contrary to most of the WAIS, after which abrupt thinning of ~400 m contributed ~1.4 – 2 m of sea level rise (Hein et al., 2016). A possible explanation for this delayed thinning in the Weddell Sea Embayment is that increased snowfall in the upper WAIS might have counteracted ice-dynamical processes at the coast until the mid-to-late Holocene (Hein et al., 2016; Spector et al., 2019). Similarly, over part of the Ross Sea sector, Neuhaus et al. (2021) showed that the grounding line over Whillans, Kamb, and Bindschadler ice streams retreated to its minimum Holocene position in the mid to late-Holocene, and then readvanced between 2 – 1 ka, coinciding with periods of warmer and colder climates, respectively. They concluded that the reported grounding-line migration was likely dominated by modest climate-induced changes upstream rather than ice dynamics further downstream, as suggested for the Weddell Sea sector (Hein et al., 2016).

Our results, which provide strong and widespread evidence for higher accumulation along the Amundsen-Weddell-Ross divide during the mid-Holocene compared with the present, support these hypotheses further, as higher accumulation rates at the divide would likely result in upstream thickening (Sect. 4.2). In the absence of ice-dynamical processes counter-balancing this increase in accumulation rates, the grounding-line should advance in these regions. However, we note that the pattern of grounding-line retreat and readvance has not been observed over the Amundsen Sea sector (Kingslake et al., 2018; Johnson et al., 2020; 2021; Braddock et al., 2022) despite the accumulation-rate increase we also observed along the Amundsen-Weddell-Ross divide and the recent results from Balco et al. (2023). This complication may indicate that the Amundsen sector is more strongly influenced by coastal changes in ice dynamics, for which even moderate changes in accumulation rate cannot compensate.

5. Conclusion

Using a ubiquitous internal reflecting horizon found across most of the Pine Island, Thwaites, and Institute and Möller ice-stream catchments, we have estimated mid-Holocene accumulation rates in the relatively slow-flowing parts of West Antarctica, representing 30% of total surface area of the WAIS.

By comparing our Holocene accumulation-rate estimates with a modern climate reanalysis model and observational syntheses, we estimated that accumulation rates across the Amundsen-Weddell-Ross Sea divide since 4.72 ka were, on average, 18% higher than modern values. Our results suggest that spatial patterns of accumulation across the WAIS have remained stable during this period, i.e. higher accumulation rates on the Amundsen side of the divide transitioning to lower accumulation rates on the Ross side of the divide. The higher accumulation rates reported here for the mid-Holocene compared to the present agree well with earlier, spatially-focused studies of accumulation rates, all of which indicate higher accumulation rates (+15 - 30%) over the past ~5 ka. This change in magnitude

563 occurred at a time of asynchronous grounding-line migration over the WAIS, including readvances of
564 the grounding line in the Weddell and Ross sectors and evidence for delayed deglaciation in the
565 Weddell Sea side of the WAIS.

566 The higher mid-Holocene accumulation estimates inferred here over large sectors of the WAIS
567 occurred at a time of sustained, millennial-scale increase in accumulation rates found at the WAIS
568 Divide Ice Core. This pattern indicates that the ice core is suitably representative of the climatic
569 conditions of the wider region over time. We suggest that future regional or continental ice-sheet
570 modelling studies base their palaeoclimate forcing on modern spatial SMB products that are
571 modulated over time using the WAIS Divide Ice Core record. This will enable those models to obtain
572 a more realistic climatic forcing representative of the past conditions of the wider WAIS, and
573 ultimately, constrain ice-sheet volume change and grounding-line evolution during the Holocene.

Code availability

575 All the codes used to produce the results presented in this paper will be made available on the
576 GitHub page of Julien A. Bodart (https://github.com/julbod, last accessed: 15 October 2022) and on
577 Zenodo (Bodart et al., 2023) upon acceptance of this manuscript.

Data availability

579 The IRH information for each of the three surveys used in this paper are archived in open-
580 access repositories (Ashmore et al., 2020b; Bodart et al., 2021b; UTIG R1 layer to be made available
581 via USAP-DC in due course) with references and links provided in the reference list. The BAS
582 airborne radar data which were used to extract the IRHs used in this paper are fully available at the
583 UK Polar Data Centre via the Polar Airborne Geophysics Data Portal (see Fremand, Bodart et al.,
584 2022). The RACMO2 product is available on request from j.m.vanwessem@uu.nl or
585 m.r.vandenbroeke@uu.nl. Links to access the observational point-based datasets used here are
586 available from the respective references mentioned in the text (Section 2.4). The gridded depth and
587 accumulation output from this study will be archived on Zenodo upon acceptance of this manuscript
588 (Bodart et al., 2023).

Author contribution

590 J.A.B. designed the study with supervision from R.G.B., D.A.Y., and D.D.B. J.A.B
591 performed the data processing, gridding, and 1-D modelling, with contributions from J.A.M. for the
592 modelling approach. J.A.B. interpreted the results with input from R.G.B., D.A.Y., D.D.B., and
593 J.A.M. J.A.B. wrote the paper, with edits from R.G.B., D.A.Y., J.A.M., D.W.A., E.Q., A.S.H.,
594 D.G.V., D.D.B.

Competing interests

596 The authors declare that they have no conflict of interest.

Acknowledgments

598 The authors would like to dedicate this work to our dear friend and colleague, Professor
599 David Vaughan, who recently passed away. This study was motivated by the AntArchitecture SCAR
600 Action Group. UTIG acknowledges the high school students who did the original AGASEA layer
601 interpretation.

Financial support

603 J.A.B. was supported by the NERC Doctoral Training Partnership grant (NE/L002558/1),
604 hosted in the Edinburgh E^3 DTP programme. J.A.B. also acknowledges the Scottish Alliance for
605 Geoscience, Environment and Society (SAGES) for funding a Postdoctoral and Early Career

Researcher Exchanges scheme to UTIG. Support for UTIG data analysis was received from NSF grant nos CDI-0941678, PLR-1443690, and PLR-10437661, as well as the G. Unger Vetlesen Foundation and the UTIG Gale White and Ewing/Worzel Fellowships. This is UTIG contribution number: xxxx (TBD).

References

Arndt, J.E., Hillenbrand, C.D., Grobe, H., Kuhn, G. and Wacker, L.: Evidence for a dynamic grounding line in outer Filchner Trough, Antarctica, until the early Holocene, Geology, 45(11), 1035-1038, https://doi.org/10.1130/G39398.1, 2017.

Ashmore, D.W., Bingham, R.G., Ross, N., Siegert, M.J., Jordan, T.A. and Mair, D.W.: Englacial architecture and age-depth constraints across the West Antarctic Ice Sheet, Geophys. Res. Lett., 47 (6), p.e2019GL086663, https://doi.org/10.1029/2019GL086663, 2020a.

Ashmore, D.W., Bingham, R.G., Ross, N., Siegert, M., Jordan, T.A. and Mair, D.W.F.:. Radiostratigraphy of the Weddell Sea sector of West Antarctica, v2.0.0, Zenodo [data set], https://doi.org/10.5281/zenodo.4945301, 2020b.

Balco, G., Brown, N., Nichols, K., Venturelli, R.A., Adams, J., Braddock, S., Campbell, S., Goehring, B., Johnson, J.S., Rood, D.H. and Wilcken, K.: Reversible ice sheet thinning in the Amundsen Sea Embayment during the Late Holocene, The Cryosphere Discussions, pp.1-24, https://doi.org/10.5194/tc-2022-172, 2022.

Beem, L.H., Young, D.A., Greenbaum, J.S., Blankenship, D.D., Cavitte, M.G., Guo, J. and Bo, S.: Aerogeophysical characterization of Titan Dome, East Antarctica, and potential as an ice core target, The Cryosphere, 15 (4), 1719-1730, https://doi.org/10.5194/tc-15-1719-2021, 2021.

Bingham, R.G. and Siegert, M.J.: Radio-echo sounding over polar ice masses. J Environ. Eng. Geoph., 12 (1), https://doi.org/10.2113/JEEG12.1.47, 47-62, 2007.

Bracegirdle, T.J., Colleoni, F., Abram, N.J., Bertler, N.A., Dixon, D.A., England, M., Favier, V., Fogwill, C.J., Fyfe, J.C., Goodwin, I. and Goosse, H.: Back to the future: Using long-term observational and palaeo-proxy reconstructions to improve model projections of Antarctic climate, Geosci. J., 9 (6), 255, https://doi.org/10.3390/geosciences9060255, 2019.

Braddock, S., Hall, B.L., Johnson, J.S., Balco, G., Spoth, M., Whitehouse, P.L., Campbell, S., Goehring, B.M., Rood, D.H. and Woodward, J.: Relative sea-level data preclude major late Holocene ice-mass change in Pine Island Bay, Nat. Geosci., 15, 568-572, https://doi.org/10.1038/s41561-022-00961-y, 2022.

Bradley, S.L., Hindmarsh, R.C., Whitehouse, P.L., Bentley, M.J. and King, M.A.: Low post-glacial rebound rates in the Weddell Sea due to Late Holocene ice-sheet readvance, Earth Planet. Sc. Lett., 413, 79-89, https://doi.org/10.1016/j.epsl.2014.12.039, 2015.

Bodart, J. A., Bingham, R. G., Ashmore, D. W., Karlsson, N.B., Hein, A. S., and Vaughan, D. G.: Age-depth stratigraphy of Pine Island Glacier inferred from airborne radar and ice core chronology, J. Geophys. Res.-Earth, 126, e2020JF005927, https://doi.org/10.1029/2020JF005927, 2021a.

Bodart, J.A., Bingham, R.G., Ashmore, D.W., Karlsson, N.B., Hein, A.S., and Vaughan, D.G.: Dated radar stratigraphy of the Pine Island Glacier catchment (West Antarctica) derived from BBAS-PASIN (2004-05) and OIB-MCoRDS2 (2016/2018) surveys, v.1.0.0, UK Polar Data Centre, Natural Environment Research Council, UK Research and Innovation [data set], https://doi.org/10.5285/F2DE31AF-9F83-44F8-9584-F0190A2CC3EB, 2021b.

Bodart, J.A., Bingham, R.G., Young, D.A., MacGregor, J.M., Ashmore, D.W., Quartini, E., Vaughan, D.G., and Blankenship D.D.: Gridded depth and accumulation products from dated airborne radar stratigraphy over West Antarctica during the mid-Holocene, v.1.0.0, Zenodo [data set], doi TBD, 2023a.

Buizert, C., Fudge, T.J., Roberts, W.H., Steig, E.J., Sherriff-Tadano, S., Ritz, C., Lefebvre, E., Edwards, J., Kawamura, K., Oyabu, I. and Motoyama, H.: Antarctic surface temperature and elevation during the Last Glacial Maximum, Science, 372 (6546), 1097-1101, https://doi.org/10.1126/science.abd2897, 2021.

Burgener, L., Rupper, S., Koenig, L., Forster, R., Christensen, W.F., Williams, J., Koutnik, M., Miege, C., Steig, E.J., Tingey, D. and Keeler, D.: An observed negative trend in West Antarctic accumulation rates from 1975 to 2010: Evidence from new observed and simulated records. J. Geophys. Res.-Atmos., 118 (10), 4205-4216, https://doi.org/10.1002/jgrd.50362, 2013.

Cavitte, M.G., Blankenship, D.D., Young, D.A., Schroeder, D.M., Parrenin, F., Lemeur, E., Macgregor, J.A. and Siegert, M.J.: Deep radiostratigraphy of the East Antarctic plateau: connecting the Dome C and Vostok ice core sites, J. Glaciol., 62 (232), 323-334, https://doi.org/10.1017/jog.2016.11, 2016.

Cavitte, M.G., Parrenin, F., Ritz, C., Young, D.A., Liefferinge, B., Blankenship, D.D., Frezzotti, M. and Roberts, J.: Accumulation patterns around Dome C, East Antarctica, in the last 73 kyr, The Cryosphere, 12, pp.1401-1414. doi: 10.5194/tc-12-1401-2018, 2018.

Cavitte, M.G., Goosse, H., Wauthy, S., Kausch, T., Tison, J.L., Van Liefferinge, B., Pattyn, F., Lenaerts, J.T. and Claeys, P.: From ice core to ground-penetrating radar: representativeness of SMB at three ice rises along the Princess Ragnhild Coast, East Antarctica, J. Glaciol., 68(272), pp.1221-1233, https://doi.org/10.1017/jog.2022.39, 2022.

Chavaillaz, Y., Codron, F. and Kageyama, M.: Southern westerlies in LGM and future (RCP4. 5) climates, Clim. Past, 9 (2), 517-524, https://doi.org/10.5194/cp-9-517-2013, 2013.

Cole-Dai, J., Ferris, D.G., Kennedy, J.A., Sigl, M., McConnell, J.R., Fudge, T.J., Geng, L., Maselli, O.J., Taylor, K.C. and Souney, J.M.: Comprehensive record of volcanic eruptions in the Holocene (11,000 years) from the WAIS Divide, Antarctica ice core, J. Geophys. Res.-Atmos., 126 (7), p.e2020JD032855, https://doi.org/10.1029/2020JD032855, 2021.

Corr, H.F., Ferraccioli, F., Frearson, N., Jordan, T., Robinson, C., Armadillo, E., Caneva, G., Bozzo, E. and Tabacco, I.: Airborne radio-echo sounding of the Wilkes Subglacial Basin, the Transantarctic Mountains and the Dome C region, Terra Ant. Rep., 13, pp.55-63. https://nora.nerc.ac.uk/id/eprint/13578 (last access: 15 October 2022), 2007.

CReSIS: CReSIS Radar Depth Sounder Data, Lawrence, Kansas, USA. Digital Media. http://data.cresis.ku.edu/ (last access: 15 October 2022), 2018.

Dansgaard, W. and Johnsen, S. J.: A flow model and a time scale for the ice core from Camp Century, Greenland, J. Glacio., 8 (53), 215–223, https://doi.org/10.3189/S0022143000031208, 1969.

Dattler, M.E., Lenaerts, J.T. and Medley, B.: Significant spatial variability in radar-derived west Antarctic accumulation linked to surface winds and topography, Geophys. Res. Lett., 46(22), pp.13126-13134, https://doi.org/10.1029/2019GL085363, 2019.

DeConto, R.M. and Pollard, D.: Contribution of Antarctica to past and future sea-level rise, Nature, 531 (7596), 591-597, https://doi.org/10.1038/nature17145, 2016.

Denton, G.H. and Hughes, T.J.: Reconstructing the Antarctic ice sheet at the Last Glacial Maximum, Quaternary Sci. Rev., 21 (1-3), 193-202, https://doi.org/10.1016/S0277-3791(01)00090-7, 2002.

Fahnestock, M., Abdalati, W., Joughin, I., Brozena, J. and Gogineni, P.: High geoSthermal heat flow, basal melt, and the origin of rapid ice flow in central Greenland, Science, 294 (5550), 2338-2342, https://doi.org/10.1126/science.1065370, 2001a.

Fahnestock, M., Abdalati, W., Luo, S. and Gogineni, S.: Internal layer tracing and age-depth-accumulation relationships for the northern Greenland ice sheet, J. Geophys. Res.-Atmos, 106(D24), pp.33789-33797, https://doi.org/10.1029/2001JD900200, 2001b.

Favier, V., Agosta, C., Parouty, S., Durand, G., Delaygue, G., Gallée, H., Drouet, A.-S., Trouvilliez, A., and Krinner, G.: An updated and quality controlled surface mass balance dataset for Antarctica, The Cryosphere, 7, 583-597, https://doi.org/10.5194/tc-7-583-2013, 2013.

Frémand, A.C., Bodart, J.A., Jordan, T.A., Ferraccioli, F., Robinson, C., Corr, H.F., Peat, H.J., Bingham, R.G. and Vaughan, D.G.: British Antarctic Survey's Aerogeophysical Data: Releasing 25 Years of Airborne Gravity, Magnetic, and Radar Datasets over Antarctica, Earth Syst. Sci. Data, 14, 3379–3410, https://doi.org/10.5194/essd-14-3379-2022, 2022.

Fudge, T.J., Markle, B.R., Cuffey, K.M., Buizert, C., Taylor, K.C., Steig, E.J., Waddington, E.D., Conway, H. and Koutnik, M.: Variable relationship between accumulation and temperature in West Antarctica for the past 31,000 years, Geophys. Res. Lett., 43(8), 3795-3803, https://doi.org/10.1002/2016GL068356, 2016.

Fudge, T. J., Buizert, C., Conway, H., and Waddington, E. D.: Accumulation Rates from the WAIS Divide Ice Core, v.1.0.0., U.S. Antarctic Program Data Center [data set], https://doi.org/10.15784/601004, 2017.

Golledge, N.R., Fogwill, C.J., Mackintosh, A.N. and Buckley, K.M.: Dynamics of the last glacial maximum Antarctic ice-sheet and its response to ocean forcing, P. Natl. Acad. Sci., 109(40), pp.16052-16056, https://doi.org/10.1073/pnas.1205385109, 2012.

Golledge, N.R., Levy, R.H., McKay, R.M., Fogwill, C.J., White, D.A., Graham, A.G., Smith, J.A., Hillenbrand, C.D., Licht, K.J., Denton, G.H. and Ackert Jr, R.P.: Glaciology and geological signature of the Last Glacial Maximum Antarctic ice sheet, Quaternary Sci. Rev., 78, pp.225-247, https://doi.org/10.1016/j.quascirev.2013.08.011, 2013

Haran, T., M. Klinger, J. Bohlander, M. Fahnestock, T. Painter, and T. Scambos: MEaSUREs MODIS Mosaic of Antarctica 2013-2014 (MOA2014) Image Map, v.1.0.0., NASA National Snow and Ice Data Center Distributed Active Archive Center [data set], https://doi.org/10.5067/RNF17BP824UM, 2018.

Harrison, C. H.: Radio Echo Sounding of Horizontal Layers in Ice, J. Glaciol., 12, 66, 383–397, https://doi.org/10.3189/S0022143000031804, 1973.

Hein, A.S., Marrero, S.M., Woodward, J., Dunning, S.A., Winter, K., Westoby, M.J., Freeman, S.P., Shanks, R.P. and Sugden, D.E.: Mid-Holocene pulse of thinning in the Weddell Sea sector of the West Antarctic ice sheet, Nat. Commun., 7 (1), 1-8, https://doi.org/10.1038/ncomms12511, 2016.

Hillenbrand, C.D., Kuhn, G., Smith, J.A., Gohl, K., Graham, A.G., Larter, R.D., Klages, J.P., Downey, R., Moreton, S.G., Forwick, M. and Vaughan, D.G.: Grounding-line retreat of the west Antarctic ice sheet from inner Pine island Bay, Geology, 41 (1), 35-38, https://doi.org/10.1130/G33469.1, 2013.

735   Hillenbrand, C.D., Bentley, M.J., Stolldorf, T.D., Hein, A.S., Kuhn, G., Graham, A.G.,
736 Fogwill, C.J., Kristoffersen, Y., Smith, J.A., Anderson, J.B. and Larter, R.D.: Reconstruction of
737 changes in the Weddell Sea sector of the Antarctic Ice Sheet since the Last Glacial Maximum,
738 Quaternary Sci. Rev., 100, 111-136, https://doi.org/10.1016/j.quascirev.2013.07.020, 2014.

739   Hillenbrand, C.D., Smith, J.A., Hodell, D.A., Greaves, M., Poole, C.R., Kender, S., Williams,
740 M., Andersen, T.J., Jernas, P.E., Elderfield, H. and Klages, J.P.: West Antarctic Ice Sheet retreat
741 driven by Holocene warm water incursions, Nature, 547 (7661), 43-48,
742 https://doi.org/10.1038/nature22995, 2017.

743   Holschuh, N., Parizek, B.R., Alley, R.B. and Anandakrishnan, S.: Decoding ice sheet
744 behavior using englacial layer slopes, Geophys. Res. Lett., 44(11), pp.5561-5570,
745 https://doi.org/10.1002/2017GL073417, 2017.

746   Holt, J. W., Blankenship, D. D., Morse, D. L., Young, D. A., Peters, M. E., Kempf, S. D.,
747 Richter, T. G., Vaughan, D. G., and Corr, H. F.: New boundary conditions for the West Antarctic Ice
748 Sheet: Subglacial topography of the Thwaites and Smith glacier catchments, Geophys. Res. Lett., 33,
749 L09502, https://doi.org/10.1029/2005GL025561, 2006.

750   IPCC: Climate Change 2021: The Physical Science Basis. Contribution of Working Group I
751 to the Sixth Assessment Report of the Intergovernmental Panel on Climate Change, edited by:
752 Masson-Delmotte, V., Zhai, P., Pirani, A., Connors, S. L., Péan, C., Berger, S., Caud, N., Chen, Y.,
753 Goldfarb, L., Gomis, M. I., Huang, M., Leitzell, K., Lonnoy, E., Matthews, J. B. R., Maycock, T. K.,
754 Waterfield, T., Yelekçi, O., Yu, R., and Zhou B., Cambridge University Press, Cambridge, United
755 Kingdom and New York, NY, USA, 147–286, https://doi.org/10.1017/9781009157896.003, in press,
756 2021.

757   Jacobel, R. W., and Welch, B. C.: A time marker at 17.5 kyr BP detected throughout West
758 Antarctica, Ann. Glaciol., 41, 47–51, https://doi.org/10.3189/172756405781813348, 2005.

759   Johnson, J.S., Bentley, M.J., Smith, J.A., Finkel, R.C., Rood, D.H., Gohl, K., Balco, G.,
760 Larter, R.D. and Schaefer, J.M.: Rapid thinning of Pine Island Glacier in the early Holocene, Science,
761 343 (6174), 999-1001, https://doi.org/10.1126/science.1247385, 2014.

762   Johnson, J.S., Roberts, S.J., Rood, D.H., Pollard, D., Schaefer, J.M., Whitehouse, P.L.,
763 Ireland, L.C., Lamp, J.L., Goehring, B.M., Rand, C. and Smith, J.A.: Deglaciation of Pope Glacier
764 implies widespread early Holocene ice sheet thinning in the Amundsen Sea sector of Antarctica, Earth
765 Planet Sc. Lett., 548, p.116501, https://doi.org/10.1016/j.epsl.2020.116501, 2020.

766   Johnson, J.S., Pollard, D., Whitehouse, P.L., Roberts, S.J., Rood, D.H. and Schaefer, J.M.:
767 Comparing glacial-geological evidence and model simulations of ice sheet change since the last
768 glacial period in the Amundsen Sea sector of Antarctica, J. Geophys. Res.-Earth, 126(6),
769 p.e2020JF005827, https://doi.org/10.1029/2020JF005827, 2021.

770   Johnson, J.S., Venturelli, R.A., Balco, G., Allen, C.S., Braddock, S., Campbell, S., Goehring,
771 B.M., Hall, B.L., Neff, P.D., Nichols, K.A. and Rood, D.H.: Existing and potential evidence for
772 Holocene grounding line retreat and readvance in Antarctica, The Cryosphere, 16 (5), 1543-1562,
773 https://doi.org/10.5194/tc-16-1543-2022, 2022.

774   Jones, R.S., Johnson, J.S., Lin, Y., Mackintosh, A.N., Sefton, J.P., Smith, J.A., Thomas, E.R.
775 and Whitehouse, P.L.: Stability of the Antarctic Ice Sheet during the pre-industrial Holocene, Nat.
776 Rev. Earth Environ., 3, 500-515, https://doi.org/10.1038/s43017-022-00309-5, 2022.

777   Karlsson, N. B., Bingham, R. G., Rippin, D. M., Hindmarsh, R. C., Corr, H. F., and Vaughan,
778 D. G.: Constraining past accumulation in the central Pine Island Glacier basin, West Antarctica, using
779 radio-echo sounding, J. Glaciol., 60, 553–562, https://doi.org/10.3189/2014JoG13j180, 2014.

780   Kausch, T., Lhermitte, S., Lenaerts, J., Wever, N., Inoue, M., Pattyn, F., Sun, S., Wauthy, S.,
781 Tison, J.L. and Van De Berg, W.J.: Impact of coastal East Antarctic ice rises on surface mass balance:
782 insights from observations and modeling, The Cryosphere, 14(10), pp.3367-3380,
783 https://doi.org/10.5194/tc-14-3367-2020, 2020.

784   Kingslake, J., Scherer, R.P., Albrecht, T., Coenen, J., Powell, R.D., Reese, R., Stansell, N.D.,
785 Tulaczyk, S., Wearing, M.G. and Whitehouse, P.L.: Extensive retreat and re-advance of the West
786 Antarctic Ice Sheet during the Holocene, Nature, 558 (7710), 430-434,
787 https://doi.org/10.1038/s41586-018-0208-x, 2018.

788   Koutnik, M.R., Fudge, T.J., Conway, H., Waddington, E.D., Neumann, T.A., Cuffey, K.M.,
789 Buizert, C. and Taylor, K.C.: Holocene accumulation and ice flow near the West Antarctic Ice Sheet
790 Divide ice core site, J. Geophys. Res.-Earth, 121 (5), 907-924. https://doi.org/10.1002/2015JF003668,
791 2016.

792   Kurbatov, A.V., Zielinski, G.A., Dunbar, N.W., Mayewski, P.A., Meyerson, E.A., Sneed,
793 S.B. and Taylor, K.C.: A 12,000 year record of explosive volcanism in the Siple Dome Ice Core, West
794 Antarctica, J. Geophys. Res.-Atmos, 111 (D12). https://doi.org/10.1029/2005JD006072, 2006.

795   Le Brocq, A.M., Bentley, M.J., Hubbard, A., Fogwill, C.J., Sugden, D.E. and Whitehouse,
796 P.L.: Reconstructing the Last Glacial Maximum ice sheet in the Weddell Sea embayment, Antarctica,
797 using numerical modelling constrained by field evidence, Quaternary Sci. Rev., 30(19-20), pp.2422-
798 2432, https://doi.org/10.1016/j.quascirev.2011.05.009, 2011.

799   Leysinger Vieli, G.J.M., Siegert, M.J. and Payne, A.J.: Reconstructing ice-sheet accumulation
800 rates at ridge B, East Antarctica, Ann. Glaciol., 39, pp.326-330,
801 https://doi.org/10.3189/172756404781814519, 2004.

802   Leysinger Vieli, G.J.M., Hindmarsh, R.C., Siegert, M.J. and Bo, S.: Time-dependence of the
803 spatial pattern of accumulation rate in East Antarctica deduced from isochronic radar layers using a 3-
804 D numerical ice flow model, J. Geophys. Res.-Earth, 116 (F2), F02018,
805 https://doi.org/10.1029/2010JF001785, 2011.

806   Leysinger Vieli, G.M., Martin, C., Hindmarsh, R.C.A. and Lüthi, M.P., Basal freeze-on
807 generates complex ice-sheet stratigraphy, Nat. Commun., 9(1), p.4669,
808 https://doi.org/10.1038/s41467-018-07083-3, 2018.

809   MacGregor, J.A., Matsuoka, K., Koutnik, M.R., Waddington, E.D., Studinger, M. and
810 Winebrenner, D.P.: Millennially averaged accumulation rates for the Vostok Subglacial Lake region
811 inferred from deep internal layers, Ann. Glaciol., 50 (51), 25-34.
812 https://doi.org/10.3189/172756409789097441, 2009.

813   MacGregor, J.A., Catania, G.A., Conway, H., Schroeder, D.M., Joughin, I., Young, D.A.,
814 Kempf, S.D. and Blankenship, D.D.: Weak bed control of the eastern shear margin of Thwaites
815 Glacier, West Antarctica, J. Glaciol., 59 (217), 900-912, https://doi.org/10.3189/2013JoG13J050,
816 2013.

817   MacGregor, J. A., Colgan, W. T., Fahnestock, M. A., Morlighem, M., Catania, G. A., Paden,
818 J. D., and Gogineni, S. P.: Holocene deceleration of the Greenland ice sheet, Science, 351 (6273),
819 590–593, https://doi.org/10.1126/science.aab1702, 2016.

MacGregor, J. A., Boisvert, L. N., Medley, B., Petty, A. A., Harbeck, J. P., Bell, R. E., Blair, J. B., Blanchard-Wrigglesworth, E., Buckley, E.,M., Christoffersen, M. S., and Cochran, J. R.: The scientific legacy of NASA's Operation Icebridge, Rev. Geophys., 59, e2020RG000712, https://doi.org/10.1029/2020RG000712, 2021.

Mayewski, P. A. and Dixon, D.A: US International TransAntarctic Scientific Expedition (US ITASE) Glaciochemical Data, v. 2.0.0., NASA National Snow and Ice Data Center [data set], http://dx.doi.org/10.7265/N51V5BXR, 2013.

Medley, B., Joughin, I., Das, S.B., Steig, E.J., Conway, H., Gogineni, S., Criscitiello, A.S., McConnell, J.R., Smith, B.E., van den Broeke, M.R. and Lenaerts, J.T.: Airborne-radar and ice-core observations of annual snow accumulation over Thwaites Glacier, West Antarctica confirm the spatiotemporal variability of global and regional atmospheric models, Geophys. Res. Lett., 40(14), pp.3649-3654, https://doi.org/10.1002/grl.50706, 2013.

Medley, B., Joughin, I., Smith, B.E., Das, S.B., Steig, E.J., Conway, H., Gogineni, S., Lewis, C., Criscitiello, A.S., McConnell, J.R. and van den Broeke, M.R.: Constraining the recent mass balance of Pine Island and Thwaites glaciers, West Antarctica, with airborne observations of snow accumulation, The Cryosphere, 8 (4), 1375-1392, https://doi.org/10.5194/tc-8-1375-2014, 2014.

Morlighem, M.: MEaSUREs BedMachine Antarctica, v.2.0.0., NASA National Snow and Ice Data Center Distributed Active Archive Center [data set], https://doi.org/10.5067/E1QL9HFQ7A8M, 2020.

Mouginot, J., Scheuchl, B., and Rignot., E.: MEaSUREs Antarctic Boundaries for IPY 2007-2009 from Satellite Radar, v.2.0.0., NASA National Snow and Ice Data Center Distributed Active Archive Center [data set], http://dx.doi.org/10.5067/AXE4121732AD, 2017.

Muldoon, G. R., Jackson, C. S., Young, D. A., and Blankenship, D. D.: Bayesian estimation of englacial radar chronology in Central West Antarctica, Dynamics and Statistics of the Climate System, 3(1), dzy004, https://doi.org/10.1093/climatesystem/dzy004, 2018.

Neuhaus, S.U., Tulaczyk, S.M., Stansell, N.D., Coenen, J.J., Scherer, R.P., Mikucki, J.A. and Powell, R.D.: Did Holocene climate changes drive West Antarctic grounding line retreat and readvance?, The Cryosphere, 15(10), 4655-4673, https://doi.org/10.5194/tc-15-4655-2021, 2021.

Neumann, T. A., Conway, H., Price, S. F., Waddington, E. D., Catania, G. A., and Morse, D. L.: Holocene accumulation and ice sheet dynamics in central West Antarctica, J. Geophys. Res.-Earth, 113 (F2), F02018, https://doi.org/10.1029/2007JF000764, 2008.

Nichols, K.A., Goehring, B.M., Balco, G., Johnson, J.S., Hein, A.S. and Todd, C.: New last glacial maximum ice thickness constraints for the Weddell Sea Embayment, Antarctica, The Cryosphere, 13(11), 2935-2951, https://doi.org/10.5194/tc-13-2935-2019, 2019.

Nielsen, L.T., Karlsson, N.B. and Hvidberg, C.S.: Large-scale reconstruction of accumulation rates in northern Greenland from radar data, Ann. Glaciol., 56(70), pp.70-78 https://doi.org/10.3189/2015AoG70A062, 2015.

Nye, J. F.: The distribution of stress and velocity in glaciers and ice-sheets, P. Roy. Soc. Lond. A. Mat., 239 (1216), 113–133. https://doi.org/10.1098/rspa.1957.0026, 1957.

Parrenin, F., Barnola, J.M., Beer, J., Blunier, T., Castellano, E., Chappellaz, J., Dreyfus, G., Fischer, H., Fujita, S., Jouzel, J. and Kawamura, K.: The EDC3 chronology for the EPICA Dome C ice core, Clim. Past, 3(3), pp.485-497, https://doi.org/10.5194/cp-3-485-2007, 2007.

Peters, M.E., Blankenship, D.D., Carter, S.P., Kempf, S.D., Young, D.A. and Holt, J.W.: Along-track focusing of airborne radar sounding data from West Antarctica for improving basal reflection analysis and layer detection, IEEE T. Geosci. Remote., https://doi.org/10.1109/TGRS.2007.897416, 45 (9), 2725-2736, 2007.

Petit, J.R., Jouzel, J., Raynaud, D., Barkov, N.I., Barnola, J.M., Basile, I., Bender, M., Chappellaz, J., Davis, M., Delaygue, G. and Delmotte, M.: Climate and atmospheric history of the past 420,000 years from the Vostok ice core, Antarctica, Nature, 399(6735), pp.429-436, https://doi.org/10.1038/20859, 1999.

Rignot, E., Mouginot, J., and Scheuchl, B.: MEaSUREs InSAR-based Antarctica ice velocity map, v.2.0.0., NASA National Snow and Ice Data Center Distributed Active Archive Center [data set], https://doi.org/10.5067/D7GK8F5J8M8R, 2017.

Ross, N., Siegert, M.J., Woodward, J., Smith, A.M., Corr, H.F., Bentley, M.J., Hindmarsh, R.C., King, E.C. and Rivera, A.: Holocene stability of the Amundsen-Weddell ice divide, West Antarctica, Geology, 39 (10), 935-938, https://doi.org/10.1130/G31920.1, 2011.

Ross, N., Bingham, R.G., Corr, H.F., Ferraccioli, F., Jordan, T.A., Le Brocq, A., Rippin, D.M., Young, D., Blankenship, D.D. and Siegert, M.J.: Steep reverse bed slope at the grounding line of the Weddell Sea sector in West Antarctica, Nat. Geosci., 5 (6), 393-396, https://doi.org/10.1038/ngeo1468, 2012.

Siegert, M.J. and Payne, A.J.: Past rates of accumulation in central West Antarctica, Geophys. Res. Lett., 31 (12), https://doi.org/10.1029/2004GL020290, 2004.

Siegert, M., Ross, N., Corr, H., Kingslake, J. and Hindmarsh, R.: Late Holocene ice-flow reconfiguration in the Weddell Sea sector of West Antarctica, Quaternary Sci. Rev., 78, 98-107, https://doi.org/10.1016/j.quascirev.2013.08.003, 2013.

Sigl, M., Toohey, M, McConnell, J.R., Cole-Dai, J., and Severi, M.: Volcanic stratospheric sulfur injections and aerosol optical depth during the Holocene (past 11 500 years) from a bipolar ice-core array, Earth Syst. Sci., 14, 3167–3196, https://doi.org/10.5194/essd-14-3167-2022, 2022.

Spector, P., Stone, J. and Goehring, B.: Thickness of the divide and flank of the West Antarctic Ice Sheet through the last deglaciation, The Cryosphere, 13 (11), 3061-3075, https://doi.org/10.5194/tc-13-3061-2019, 2019.

Sproson, A.D., Yokoyama, Y., Miyairi, Y., Aze, T. and Totten, R.L.: Holocene melting of the West Antarctic Ice Sheet driven by tropical Pacific warming, Nat. Commun., 13 (1), 1-9, https://doi.org/10.1038/s41467-022-30076-2, 2022.

Steig, E.J., Fastook, J.L., Zweck, C., Goodwin, I.D., Licht, K.J., White, J.W. and Ackert Jr, R.P.: West Antarctic ice sheet elevation changes, The West Antarctic Ice Sheet: Behavior and Environment, 77, 75-90. https://doi.org/10.1029/AR077p0075, 2001.

Stone, J.O., Balco, G.A., Sugden, D.E., Caffee, M.W., Sass III, L.C., Cowdery, S.G. and Siddoway, C.: Holocene deglaciation of Marie Byrd land, west Antarctica, Science, 299 (5603), 99-102, https://doi.org/10.1126/science.1077998, 2003.

Suganuma, Y., Miura, H., Zondervan, A. and Okuno, J.I.: East Antarctic deglaciation and the link to global cooling during the Quaternary: Evidence from glacial geomorphology and 10Be surface exposure dating of the Sør Rondane Mountains, Dronning Maud Land, Quaternary Sci. Rev., 97, pp.102-120, https://doi.org/10.1016/j.quascirev.2014.05.007, 2014.

904 Sutter, J., Fischer, H. and Eisen, O.: Investigating the internal structure of the Antarctic ice
905 sheet: the utility of isochrones for spatiotemporal ice-sheet model calibration, The Cryosphere, 15 (8),
906 3839-3860. https://doi.org/10.5194/tc-15-3839-2021, 2021.

907 RAISED Consortium: A community-based geological reconstruction of Antarctic Ice Sheet
908 deglaciation since the Last Glacial Maximum, Quaternary Sci. Rev., 100, pp.1-9,
909 https://doi.org/10.1016/j.quascirev.2014.06.025, 2014.

910 Van Den Broeke, M.R. and Van Lipzig, N.P.: Changes in Antarctic temperature, wind and
911 precipitation in response to the Antarctic Oscillation, Ann. Glaciol, 39, 119-126,
912 https://doi.org/10.3189/172756404781814654, 2004.

913 Van Wessem, J.M., Van De Berg, W.J., Noël, B.P., Van Meijgaard, E., Amory, C., Birnbaum,
914 G., Jakobs, C.L., Krüger, K., Lenaerts, J., Lhermitte, S. and Ligtenberg, S.R.: Modelling the climate
915 and surface mass balance of polar ice sheets using RACMO2–Part 2: Antarctica (1979–2016), The
916 Cryosphere, 12 (4), 479-1498, https://doi.org/10.5194/tc-12-1479-2018, 2018.

917 Vaughan, D.G., Corr, H.F., Ferraccioli, F., Frearson, N., O'Hare, A., Mach, D., Holt, J.W.,
918 Blankenship, D.D., Morse, D.L. and Young, D.A.: New boundary conditions for the West Antarctic
919 ice sheet: Subglacial topography beneath Pine Island Glacier, Geophys. Res. Lett., 33 (9), L09501,
920 https://doi.org/10.1029/2005GL025588, 2006.

921 Venturelli, R.A., Siegfried, M.R., Roush, K.A., Li, W., Burnett, J., Zook, R., Fricker, H.A.,
922 Priscu, J.C., Leventer, A. and Rosenheim, B.E.: Mid-Holocene grounding line retreat and readvance
923 at Whillans Ice Stream, West Antarctica, Geophys. Res. Lett., 47 (15), p.e2020GL088476,
924 https://doi.org/10.1029/2020GL088476, 2020.

925 Waddington, E. D., Neumann, T. A., Koutnik, M. R., Marshall, H.-P., and Morse, D. L.:
926 Inference of accumulation-rate patterns from deep layers in glaciers and ice sheets, J. Glaciol., 53
927 (183), 694–712, https://doi.org/10.3189/002214307784409351, 2007.

928 WAIS Divide Project Members: Onset of deglacial warming in West Antarctica driven by
929 local orbital forcing, Nature, 500 (7463), 440-444, https://doi.org/10.1038/nature12376, 2013.

930 Wearing, M.G. and Kingslake, J.: Holocene Formation of Henry Ice Rise, West Antarctica,
931 Inferred from Ice-Penetrating Radar, J. Geophys. Res.-Earth, 124 (8), 2224-2240,
932 https://doi.org/10.1029/2018JF004988, 2019.

933 Whillans, I. M.: Radio-echo layers and the recent stability of the West Antarctic ice sheet,
934 Nature, 264, 5582, 152, https://doi.org/10.1038/264152a0, 1976.

935 Winter, A., Steinhage, D., Creyts, T.T., Kleiner, T. and Eisen, O.: Age stratigraphy in the East
936 Antarctic Ice Sheet inferred from radio-echo sounding horizons, Earth Syst. Sci. Data, 11 (3), 1069-
937 1081, https://doi.org/10.5194/essd-11-1069-2019, 2019.

938